“National Adaptation Plan (NAP) to advance medium and long-term adaptation planning in Armenia”

UNDP-GCF/00104267 Project

Remote-Sensing based Assessment of Evapotranspiration and Forecasted Projections

Prepared by: Aleksandr Arakelyan, National Expert on Water Resources Climate Risk and Vulnerability Assessment

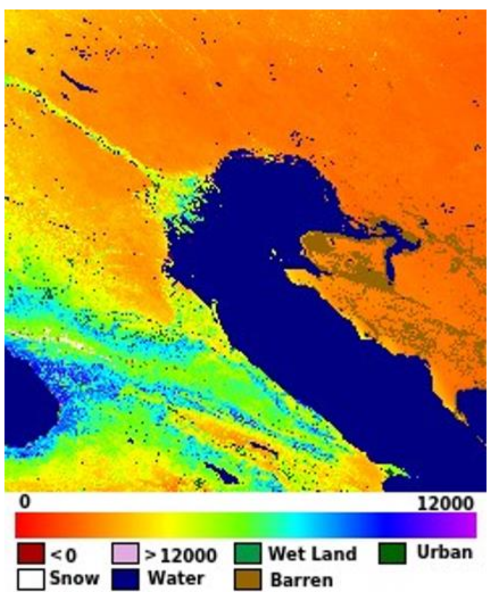

Yerevan, Armenia

December 2020

Contents

List of Tables

List of Figures

1. Introduction: Actual and Potential Evapotranspiration

Monitoring and estimating of evapotranspiration (ET) is vital and necessary for allocating and managing water resources in agricultural areas, especially in arid and semi-arid climates. Assessment of water used by crops can be conducted over large agricultural areas using satellites images and products (Salehnia et al., 2018).

There are two different aspects of evapotranspiration: potential evapotranspiration and actual evapotranspiration.

Potential evapotranspiration (PE, PET) is a measure of the ability of the atmosphere to remove water from the surface through the processes of evaporation and transpiration assuming no control on water supply. Actual evapotranspiration (AE) is the quantity of water that is actually removed from a surface due to the processes of evaporation and transpiration.

Scientists consider these two types of evapotranspiration for the practical purpose of water resource management. Around the world humans are involved in the production of a variety of plant crops. Many of these crops grow in environments that are naturally short of water. As a result, irrigation is used to supplement the crop's water needs. Managers of these crops can determine how much supplemental water is needed to achieve maximum productivity by estimating potential and actual evapotranspiration. Estimates of these values are then used in the following equation:

crop water need = potential evapotranspiration - actual evapotranspiration

The following factors are extremely important in estimating potential evapotranspiration:

Potential evapotranspiration requires energy for the evaporation process. The major source of this energy is from the Sun. The amount of energy received from the Sun accounts for 80% of the variation in potential evapotranspiration.

Wind is the second most important factor influencing potential evapotranspiration. Wind enables water molecules to be removed from the ground surface by a process known as eddy diffusion.

The rate of evapotranspiration is associated to the gradient of vapor pressure between the ground surface and the layer of atmosphere receiving the evaporated water (Pidwirny, 2006).

2. Estimation of Evapotranspiration using MODIS Global Evapotranspiration Project (MOD16)

2.1 MOD16 Global Evapotranspiration Product

This project is part of NASA/EOS project to estimate global terrestrial evapotranspiration from Earth land surface by using satellite remote sensing data.

Computing ET is a combination of two complicated major issues: (1) estimating the stomatal conductance to derive transpiration from plant surfaces; and (2) estimating evaporation from the ground surface. The MOD16 ET algorithm runs at daily basis and temporally, daily ET is the sum of ET from daytime and night. Vertically, ET is the sum of water vapor fluxes from soil evaporation, wet canopy evaporation and plant transpiration at dry canopy surface.

MOD16 global evapotranspiration product can be used to calculate regional water and energy balance, soil water status; hence, it provides key information for water resource management. With long-term ET data, the effects of changes in climate, land use, and ecosystems disturbances (e.g. wildfires and insect outbreaks) on regional water resources and land surface energy change can be quantified.

The MOD16 global evapotranspiration (ET)/latent heat flux (LE)/potential ET (PET)/potential LE (PLE) datasets are regular 1-km^2 land surface ET datasets for the 109.03 Million km^2 global vegetated land areas at 8-day, monthly and annual intervals. The dataset covers the time period from 2000 to present (Figure 1).

The MOD16 ET datasets are estimated using Mu et al.'s improved ET algorithm (2011) over previous Mu et al.s paper (2007a). The ET algorithm is based on the Penman-Monteith equation (Monteith, 1965). Surface resistance is an effective resistance to evaporation from land surface and transpiration from the plant canopy.

Terrestrial ET includes evaporation from wet and moist soil, from rain water intercepted by the canopy before it reaches the ground, and the transpiration through stomata on plant leaves and stems. Evaporation of water intercepted by the canopy is a very important water flux for ecosystems with a high LAI. Canopy conductance for plant transpiration is calculated by using LAI to scale stomatal conductance up to canopy level. For many plant species during growing seasons, stomatal conductance is controlled by vapor pressure deficit (VPD) (Oren et al., 1999; Mu et al., 2007b; Running Kimball, 2005) and daily minimum air temperature (T_{min}). T_{min} is used to control dormant and active growing seasons for evergreen biomes. High temperatures are often accompanied by high VPDs, leading to partial or complete closure of stomata. For a given biome type, two threshold values for T_{min} and VPD are listed in the Biome-Property-Look-Up-Table (BPLUT) to control stomatal conductance (Mu et al., 2007a; 2009; 2011).

MOD16 products includes 8-day, monthly and annual ET, LE, PET, PLE and 8-day, annual quality control (ET_QC). The 8-day MOD16A2 QC field is inherited from MOD15A2 in the same period (Running et al., 2019).

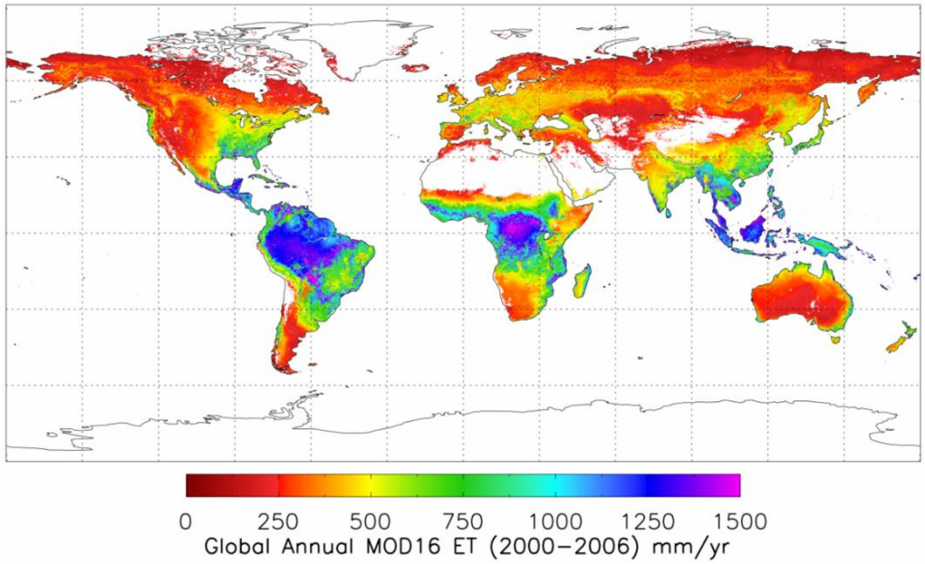

Figure 1. Global Annual Evapotranspiration (2000-2006) mm/yr, MOD16 Dataset

2.2 Penman–Monteith method

Developing a robust algorithm to estimate global evapotranspiration is a significant challenge. Traditional energy balance models of ET require explicit characterization of numerous physical parameters, many of which are difficult to determine globally. For these models, thermal remote sensing data (e.g., land surface temperature, LST) are the most important inputs. However, using the 8-day composite MODIS LST (the average LST of all cloud-free data in the compositing window) (Wan et al., 2002) and daily meteorological data recorded at the flux tower, Cleugh et al. (2007) demonstrate that the results from thermal models are unreliable at two Australian sites (Virginia Park, a wet/dry tropical savanna located in northern Queensland and Tumbarumba, a cool temperate, broadleaved forest in south east New South Wales). Using a combination of remote sensing and global meteorological data, developers of MOD16 dataset have adapted the Cleugh et al. (2007) algorithm, which is based on the Penman–Monteith method and calculates both canopy conductance and ET.

Monteith (1965) gave the following equation:

$$\lambda E = \frac{s\,A' + \rho\,C_p \frac{(e_{sat} - e)}{r_a}}{s + \gamma\left(1 + \frac{r_s}{r_a}\right)} = \frac{s\,A' + \rho\,C_p \frac{VPD}{r_a}}{s + \gamma\left(1 + \frac{r_s}{r_a}\right)} \qquad (1)$$

where $s = d(e_{sat})/T$, the slope of the curve relating saturated water vapor pressure (e_{sat}) to temperature; A′ is available energy partitioned between sensible heat and latent heat fluxes on land surface. VPD = $e_{sat} - e$ is the air vapor pressure deficit. All inputs have been previously defined except for surface resistance r_s, which is an effective resistance accounting for evaporation from the soil surface and transpiration from the plant canopy.

Despite its theoretical appeal, the routine implementation of the Penman–Monteith equation is often hindered by requiring meteorological forcing data (A', T_a and VPD) and the aerodynamic and surface resistances (r_a and r_s). Radiation and soil heat flux measurements are needed to determine A′; air temperature and humidity to calculate VPD; and wind speed and surface roughness parameters to determine r_a. Multi-temporal implementation of the Penman–Monteith model at regional scales requires routine surface meteorological observations of air temperature, humidity, solar radiation and wind speed. Models for estimating maximum stomatal conductance including the effect of limited soil water availability and stomatal physiology requires either a fully coupled biophysical model such as that by Tuzet et al. (2003) or resorting to the empirical discount functions of Jarvis (1976), which must be calibrated. Determining a surface resistance for partial canopy cover is even more challenging with various dual source models proposed (e.g., Shuttleworth and Wallace, 1985) to account for the presence of plants and soil (Running et al., 2019)..

2.3 The MOD16A2/MOD16A3 algorithm logic

MOD16 ET algorithm is based on the Penman-Monteith equation (Monteith, 1965) as in equation 1. Figure 1 shows the logic behind the improved MOD16 ET Algorithm for calculating daily MOD16 ET algorithm (Running et al., 2019).

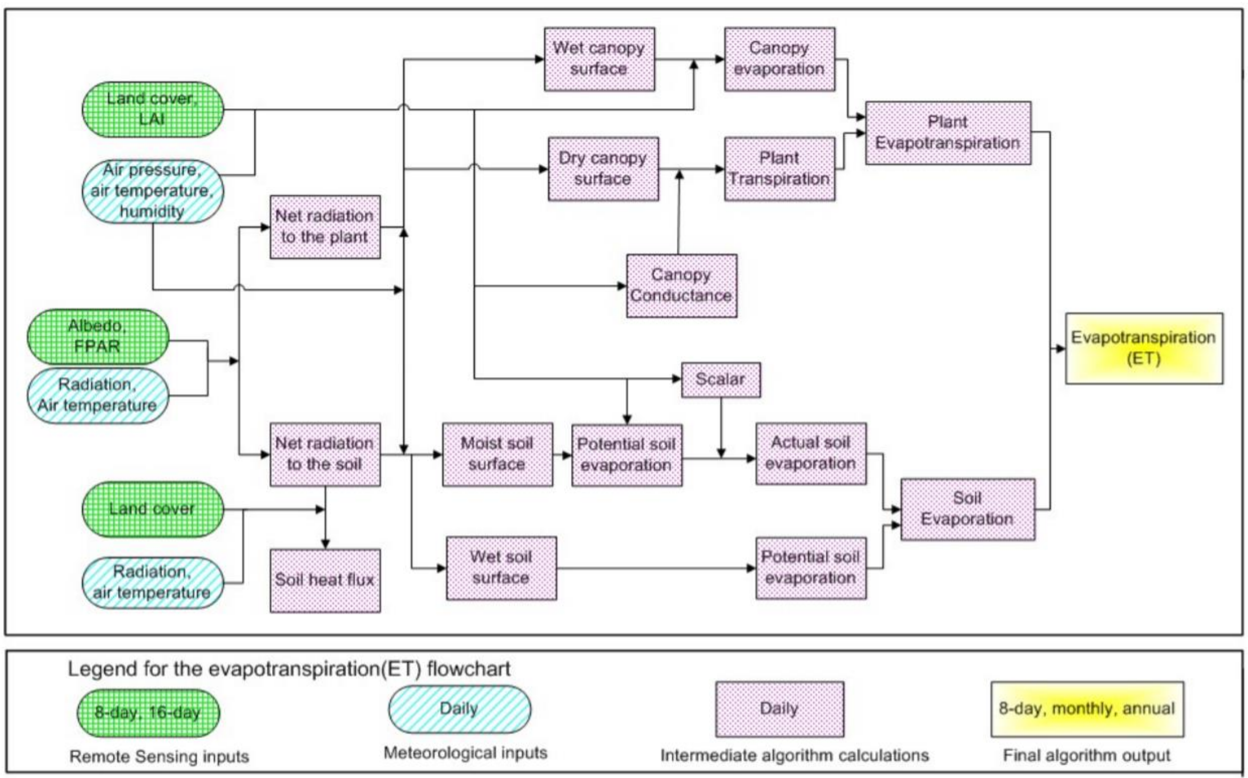

Figure 2. Flowchart of the improved MOD16 ET algorithm. LAI - leaf area index; FPAR - Fraction of Photosynthetically Active Radiation.

2.3.1 Dependence of ET from MODIS Land Cover Classification

One of the most important inputs of MOD16 algorithm is MODIS Land Cover Product. MOD16 algorithm uses the lan cover classification based on the Biome Properties Look-Up Table (BPLUT).

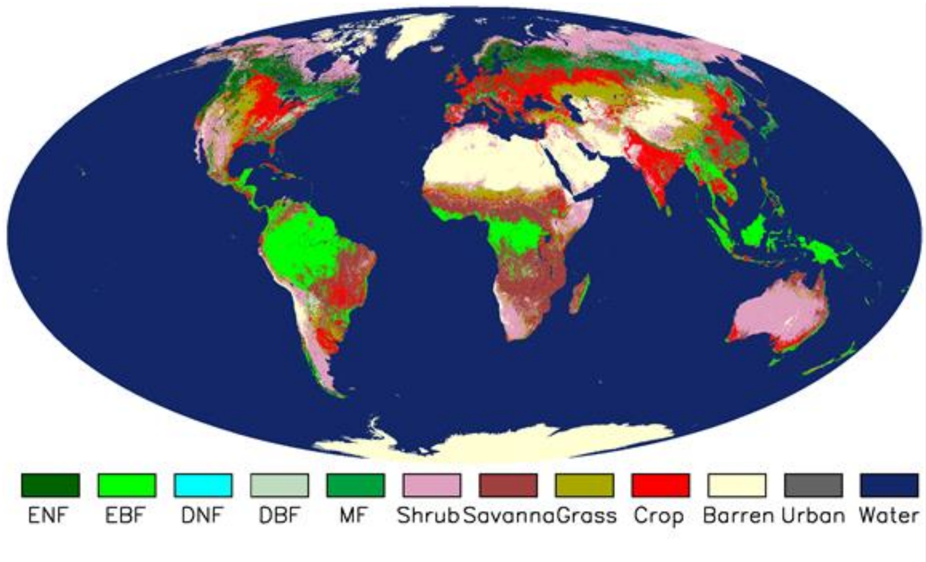

Figure 3. MODIS Land Cover Classification Scheme (MCDLCHKM)

Table 1. The land cover types used in the MOD16 Algorithm

Class Value	Class Description
0	Water
1	Evergreen Needleleaf Forest
2	Evergreen Broadleaf Forest
3	Deciduous Needleleaf Forest
4	Deciduous Broadleaf Forest
5	Mixed Forest
6	Closed Shrubland
7	Open Shrubland
8	Woody Savanna
9	Savanna
10	Grassland
12	Cropland
13	Urban or Built-Up
16	Barren or Sparsely Vegetated
254	Unclassified
255	Missing Data

2.3.2 GMAO daily meteorological data

The MOD16 algorithm computes ET at a daily time step. This is made possible by the daily meteorological data, including average and minimum air temperature, incident PAR and specific humidity, provided by NASA's Global Modeling and Assimilation Office (GMAO or MERRA GMAO), a branch of NASA (Schubert et al. 1993). These data, produced every six hours, are derived using a global circulation model (GCM), which incorporates both ground and satellite-based observations. These data are distributed at a resolution of 0.5° x 0.6° (MERRA GMAO) or 1.00° x 1.25° in contrast to the 0.5 km gridded MOD16 outputs. It is assumed that the coarse resolution meteorological data provide an accurate depiction of ground conditions and are homogeneous within the spatial extent of each cell.

One major problem is the inconsistency in spatial resolution between half-degree GMAO/NASA meteorological data and 0.5 km MODIS pixel. The authors of MOD16A product solved the problem by spatially smoothing meteorological data to 0.5 km MODIS pixel level. For the problem arising from coarse spatial resolution daily GMAO data, we use spatial interpolation to enhance meteorological inputs. The four GMAO cells nearest to a given 0.5 km MODIS pixel are used in the interpolation algorithm. There are two reasons for choosing four GMAO cells per 0.5 km MODIS pixel: (1) this will not slow down the computational efficiency of creating MOD16, which is a global product, and (2) it is more reasonable to assume no elevation variation within four GMAO cells than more GMAO cells (Running et al., 2019).

Theoretically, this GMAO spatial interpolation can improve the accuracy of meteorological data for each 0.5 km pixel because it is unrealistic for meteorological data to abruptly change from one side of GMAO boundary to the other. To explore the above question the authors use observed daily weather data from World Meteorological Organization (WMO) daily surface observation network (>5000 stations) to compare changes in Root Mean Squared Error (RMSE) and Correlation (COR) between the original and enhanced DAO data. As a result of the smoothing process, on average, RMSE is reduced and COR increased for 72.9% and 84% of the WMO stations, respectively, when comparing original and enhanced DAO data to WMO observations for 2001 and 2002. Clearly, the nonlinear spatial interpolation significantly improves GMAO inputs for most stations, although for a few stations, interpolated GMAO accuracy may be reduced due to the inaccuracy of GMAO in these regions. (Zhao et al. 2005, 2006).

2.4 Description of MOD16 Data Sets

There are two major MOD16 data sets, 8-day composite MOD16A2 and annual composite MOD16A3. Both MOD16A2 and MOD16A3 are stored in HDFEOS2 scientific data file format (http://hdfeos.org/software/library.php). HDFEOS2 file format is an extension of HDF4 by adding geo-reference, map projection, and other key meta data information to HDF4 format (https://support.hdfgroup.org/products/hdf4/) to facilitate users to use satellite data products from NASA's Earth Observing System (EOS) projects. Since MOD16 is a level 4 EOS data product, the grid data sets are saved in Sinusoidal (SIN) map projection, an equal-area map projection, with an earth radius of 6371007.181 meters (the inversed lat/lon are in WGS84 datum). The MODIS high-level data sets divide the global SIN into many chunks, so-called 10-degree tiles (https://modis-land.gsfc.nasa.gov/MODLAND_grid.html). There are 317 land tiles, and among which, 300 tiles (286 tiles for the Collection5) located within latitude of 60°S and 90°N (90°N for the Collection5) have vegetated land pixels. Therefore, for each 8-day Collection6 MOD16A2 and yearly MOD16A3, there are 300 land tiles globally if there are no missing tiles.

When MODIS updates MOD16 from the Collection5 to Collection6, the spatial resolution has increased from nominal 1-km (926.62543313883 meters) to 500m (463.312716569415 meters), to be consistent with changes in the spatial resolution of a major input to MOD16, the 8-day MOD15A2H.

In our assessments for Armenia, we used MOD16A3 product. Table 2 presents science data sets in annual MOD16A3 (or MOD16A3GF). ET_500m and PET_500m are the ***summation*** of total daily ET/PET through the year (0.1 kg/m2/year) whereas LE and PLE are the corresponding ***average*** total latent energy over a unit area for a unit day (10000 J/m2/day) through the year. LE_500m and PLE_500m have the same unit, data type (signed 2-byte short int16), valid range and fill values as those listed above for the 8-day MOD16A2; whereas annual ET_500m and PET_500m are saved in unsigned 2-byte short integer (uint16) with valid range from 0 to 65528.

The real value (Real_value) of each data set (ET, LE, PET or PLE) in the corresponding units (kg/m2/yr or J/m2/d) can be calculated using the following equation:

Real_value = Valid_data x Scale_Factor

Table 2. The detailed information on science data sets in MOD16A3 (or MOD16A3GF)

Data Sets	Meaning	Units	Date Type	Valid Range	Scale Factor
ET_500m	annual sum ET	$kg/m^2/yr$	uint16	0 ~ 65528	0.1
LE_500m	annual average LE	$J/m^2/d$	int16	0 ~ 32760	10000
PET_500m	annual sum PET	$kg/m^2/yr$	uint16	0 ~ 65528	0.1
PLE_500m	annual average PLE	$J/m^2/d$	int16	0 ~ 32760	10000
ET_QC_500m	Quality Assessment	Percent (%)	uint8	0 ~ 100	none

All MODIS land data products are distributed to global users from the USGS Land Processes Distributed Active Archive Center (USGS LP DAAC), found here: https://lpdaac.usgs.gov/. Specific details about the MODIS land products can be found here: https://lpdaac.usgs.gov/dataset_discovery/modis, including details about sensor spectral bands, spatial/temporal resolution, platform overpass timing, datafile naming conventions, tiling formats, processing levels and more.

MODIS data can be downloaded from NASA EarthData Search portal: https://search.earthdata.nasa.gov/

EarthData Search provides the only means for data discovery, filtering, visualization, and access across all of NASA's Earth science data holdings. It allows to search by any topic, collection, or place name. Using Global Imagery Browse Services (GIBS), EarthData Search enables high-performance, highly available data visualization when applicable.

3. ET and PET Calculation for the Territory of Armenia

3.1 Downloading the datasets for Armenia

In the EarthData Search, it is necessary to select area for which the data is need to be downloaded. In the image below, the territory of Armenia is selected by rectangle. We can see that the territory of Armenia is distributed within two tiles. For all 20 years of observations (2000-2019), we have 40 images in total.

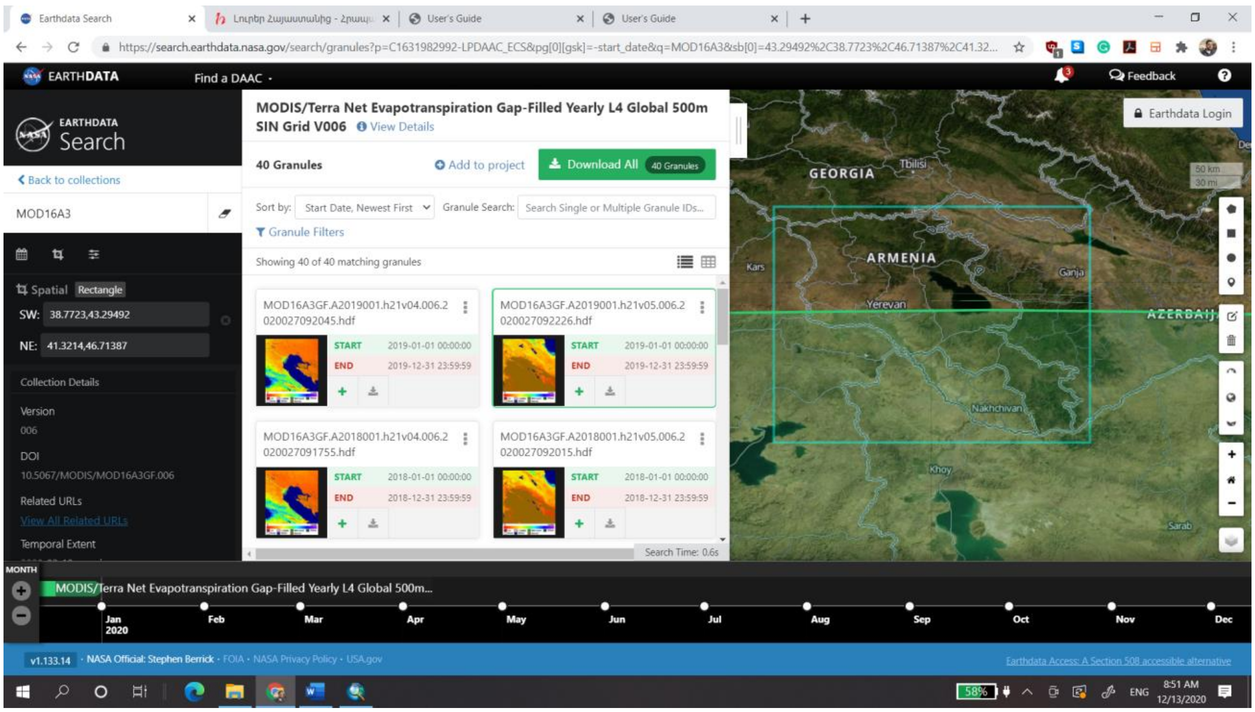

Figure 4. Downloading the MOD16A3 Product for the Territory of Armenia

3.2 Data preprocessing

After downloading all images, we need to preprocess them in order to be able to calculate ET and PET for Armenia and separate sub-basins.

MODIS files downloaded from EarthData are initially in hdf format with Sinusoidal Coordinate System. In ESRI ArcGIS environment, it is possible to save these files in GeoTIFF format with WGS84 coordinate system.

After that, it is necessary to merge two tiles for each year and extract the ET/PET raster by the shapefile of Armenia.

In the MOD16A3 data sets, there are 7 fill values as listed below for non-vegetated pixels without ET/PET calculations:

65535 = _Fill value
65534 = land cover assigned as perennial salt or Water bodies

65533 = land cover assigned as barren, sparse veg (rock, tundra, desert) (A3/A3GF), also used for data gaps from cloud cover and snow for vegetated pixels (A3)
65532 = land cover assigned as perennial snow,ice.
65531 = land cover assigned as "permanent" wetlands/inundated marshland
65530 = land cover assigned as urban/built-up
65529 = land cover assigned as "unclassified" or (not able to determine)

Before calculating the ET/PET for the territory of Armenia, it is necessary to remove these values. In our case, we performed that using the SetNull tool of ArcGIS Spatial Analyst extension.

As it mentioned in MOD16A3 product description, the scale factor of ET and PET data sets is 0.1. It means that if we want to get the real values in mm/year for each pixel, we need to multiply the raster with 0.1.

$$\text{Real\_value} = \text{Valid\_data} \times \text{Scale\_Factor}$$

3.3 ET and PET calculation

In order to get the ET/PET values for each pixel in million cubic meters, we should multiply the pixel value with the cell area:

$$\text{ET(PET), million } m^3 = \text{Real value, mm } /1000 \times (463.312716569415 \text{ m} \times 463.312716569415 \text{ m}) / 1000000$$

Using the Zonal Statistics tool, the ET/PET data were calculated for the sub-basins that have been used for the vulnerability assessment of water resources due to the climate change (see the vulnerability map in the first report).

As we needed to perform the above-mentioned steps for 40 times (20 years x 2 (ET+PET)), we created a model through Model Builder to automate this process (Figure 5).

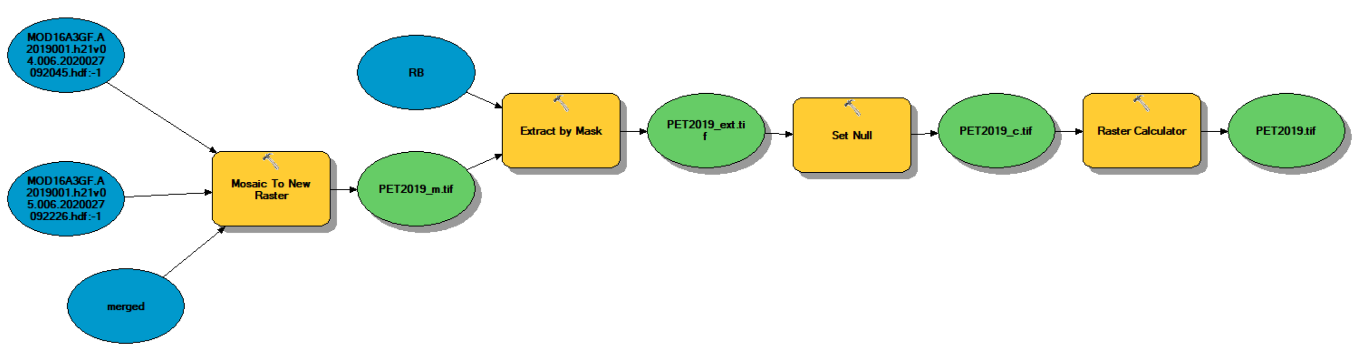

Figure 5. Model for Calculation of Annual ET/PET Values for the Sub-basins in Armenia

3.4 Results

The output of the model is the ET/PET raster for each year (2000-2019, 40 data sets). Each pixel of the raster represents the annual value of evapotranspiration from that cell in million cubic meters.

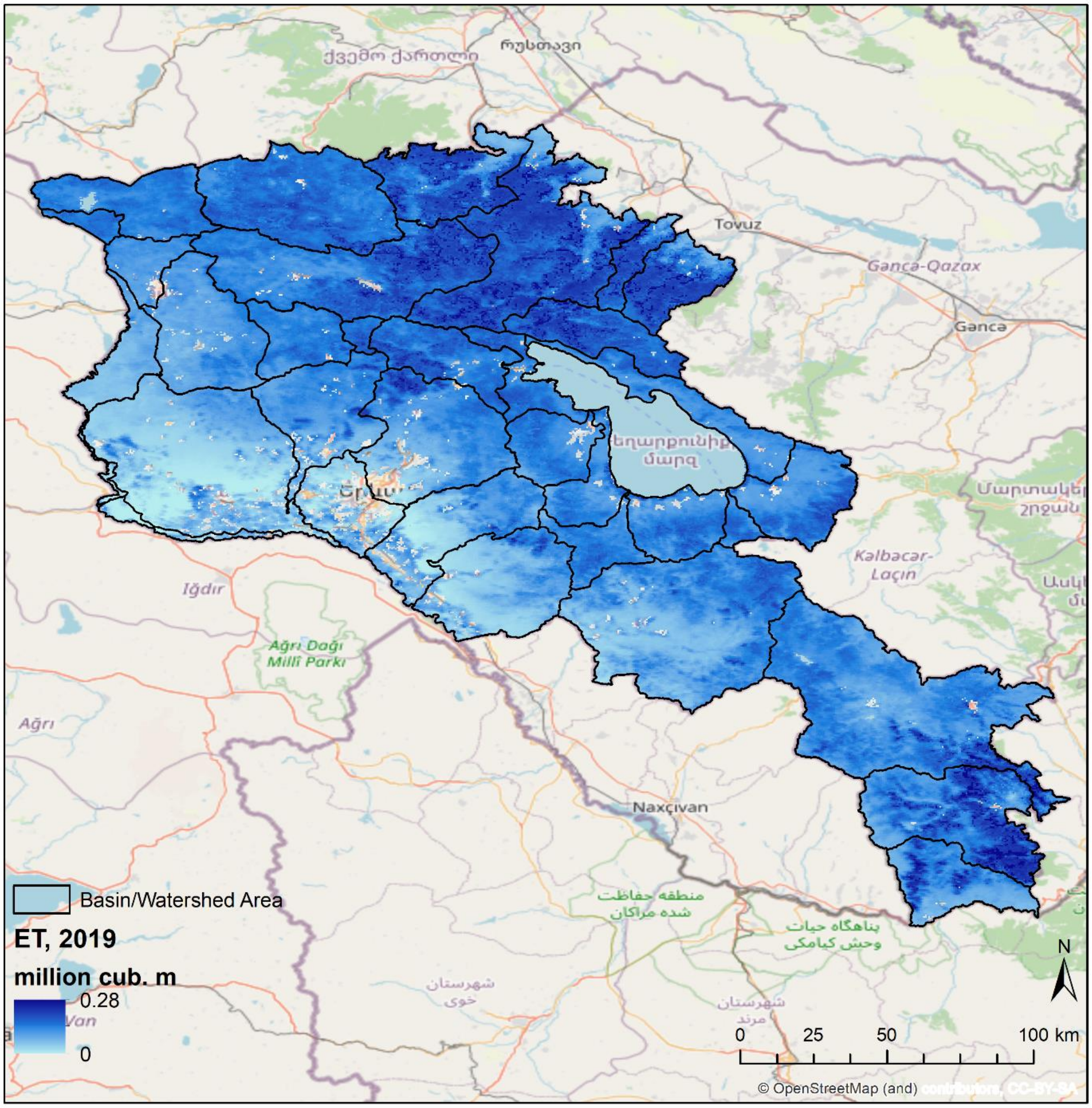

Figure 6. Actual Evapotranspiration Raster Dataset for the Territory of Armenia (2019)

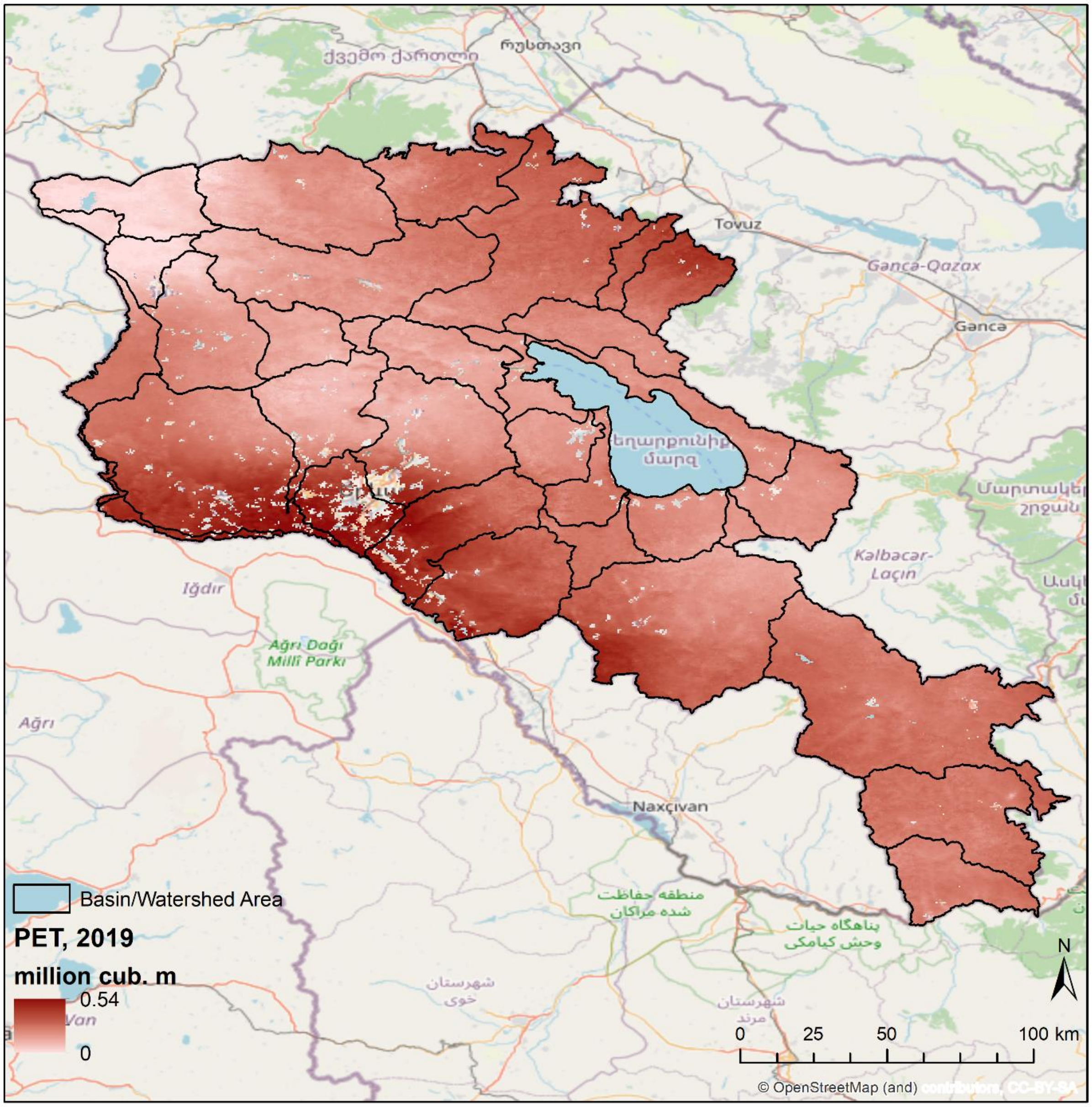

Figure 7. Actual Evapotranspiration Raster Dataset for the Territory of Armenia (2019)

As we can see from the Figures 6 and 7, the highest values of actual evapotranspiration are observed in the more densely vegetated territories (specifically in forested areas), and the highest values of potential evapotranspiration are in the territories with highest annual average temperatures.

Using the Zonal Statistics tool, the ET and PET values have been aggregated for the sub-basins delineated in the water resources vulnerability assessment. The results are presented in the table below and in the Annex 1.

*Table 3. Annual Values of ET and PET for the Sub-basins Delineated in Armenia (average for 2000-2019, million cub. m)**

Sub-basin	ET, Avg for 2000-2019	PET, Avg for 2000-2019
r. Pambak	1028.1	2206.0
r. Aghstev	1214.5	2642.2
r. Sevjur	707.1	3404.1
Lake Sevan	10.9	31.8
r. Azat	358.4	1516.4
r. Vedi	414.1	1799.8
r. Arpa	1052.3	3463.2
r. Tavush, Hakhindja	342.3	824.0
r. Vorotan	1376.9	3905.2
r. Voghji	725.5	1870.0
r. Meghriget	315.6	987.5
r. Dzoraget	871.0	1808.5
r. Debed	528.4	1171.9
r. Getik	385.7	809.2
r. Hakhum	155.1	365.3
r. Araks	34.4	216.9
r. Dzknaget, north-western shore of Lake Sevan	198.1	450.9
r. Gavaraget	257.4	640.8
r. Masrik	370.9	955.5
Eastern shore of Lake Sevan	294.6	801.9
Western and south-western shore of Lake Sevan	192.2	543.6
Southern shore of Lake Sevan	265.7	700.4
Lower flow of Hrazdan River	133.1	710.7
Middle flow of Hrazdan River	574.7	1661.8
Upper flow of Hrazdan River	352.0	783.5
Upper flow of Kasakh River	257.0	614.1
Lower flow of Akhuryan River	242.1	824.4
Middle flow of Akhuryan River	142.5	348.5
Upper flow of Akhuryan River	404.3	812.1
Middle and lower flows of Kasakh River	425.3	1161.3
r. Mantash (Karkachun)	464.6	1321.2
r. Marmarik	53.1	112.2
r. Karchaghbyur	60.9	150.7
r. Argichi	198.2	549.3
ARMENIA	14407.3	40164.7

**values for each year are presented in the Annex 1.*

In the table below, calculated values of annual actual and potential evapotranspiration for Armenia are presented.

Table 4. Calculated Values of Annual Actual and Potential Evapotranspiration for Armenia, 2000-2019

Year	ET	PET
2000	11679.2	42485.7
2001	12023.0	42056.3
2002	13876.6	39838.1
2003	14252.7	37020.7
2004	13980.2	40861.8
2005	14484.5	39214.1
2006	14085.8	40849.2
2007	15453.0	38275.3
2008	14108.6	40961.3
2009	15049.8	36793.6
2010	15252.3	41968.4
2011	15525.7	36763.0
2012	14705.0	38932.1
2013	15089.8	40136.1
2014	14464.3	41569.0
2015	14614.4	41499.7
2016	15744.4	39472.9
2017	14121.0	43499.9
2018	15229.4	40932.4
2019	14456.0	42011.2

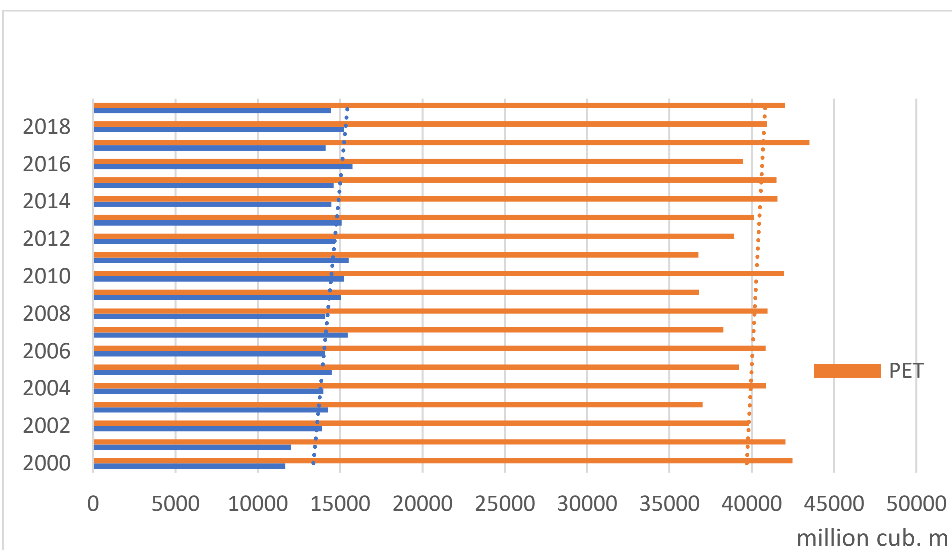

Figure 8. Annual Actual and Potential Evapotranspiration for Armenia, 2000-2019

Actual evapotranspiration estimations for 2000-2015 are also included in UNSD/UNEP (United Nations Statistics Division, United Nations Environmental Program) Environmental Indicators database. This country-level data is available through UNData portal: http://data.un.org/Data.aspx?d=ENV&f=variableID%3A7.

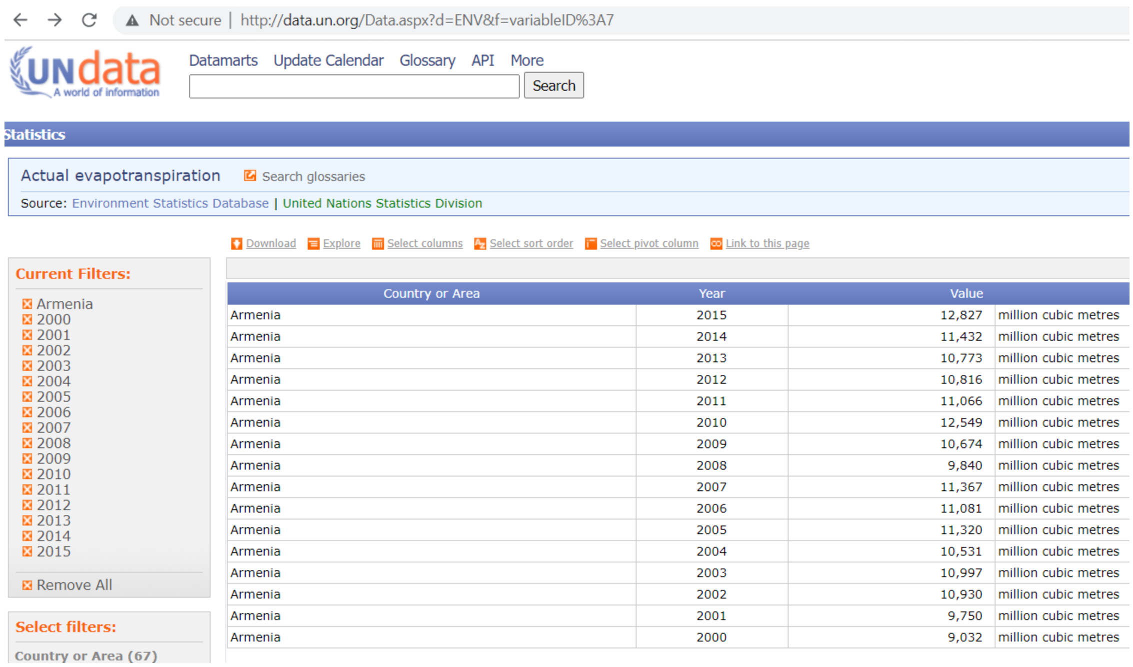

Not secure | http://data.un.org/Data.aspx?d=ENV&f=variableID%3A7

UNdata A world of information

Datamarts Update Calendar Glossary API More

Search

Statistics

Actual evapotranspiration   Search glossaries

Source: Environment Statistics Database | United Nations Statistics Division

Download Explore Select columns Select sort order Select pivot column Link to this page

Current Filters:

Armenia
2000
2001
2002
2003
2004
2005
2006
2007
2008
2009
2010
2011
2012
2013
2014
2015

Remove All

Select filters:

Country or Area (67)

Country or Area	Year	Value	
Armenia	2015	12,827	million cubic metres
Armenia	2014	11,432	million cubic metres
Armenia	2013	10,773	million cubic metres
Armenia	2012	10,816	million cubic metres
Armenia	2011	11,066	million cubic metres
Armenia	2010	12,549	million cubic metres
Armenia	2009	10,674	million cubic metres
Armenia	2008	9,840	million cubic metres
Armenia	2007	11,367	million cubic metres
Armenia	2006	11,081	million cubic metres
Armenia	2005	11,320	million cubic metres
Armenia	2004	10,531	million cubic metres
Armenia	2003	10,997	million cubic metres
Armenia	2002	10,930	million cubic metres
Armenia	2001	9,750	million cubic metres
Armenia	2000	9,032	million cubic metres

Figure 9. Annual Actual Evapotranspiration Values for Armenia, 2000-2015 (UNSD/UNEP)

As we can see from the graph below, the values estimated by UNSD/UNEP are smaller than the values obtained from MODIS MOD16 product.

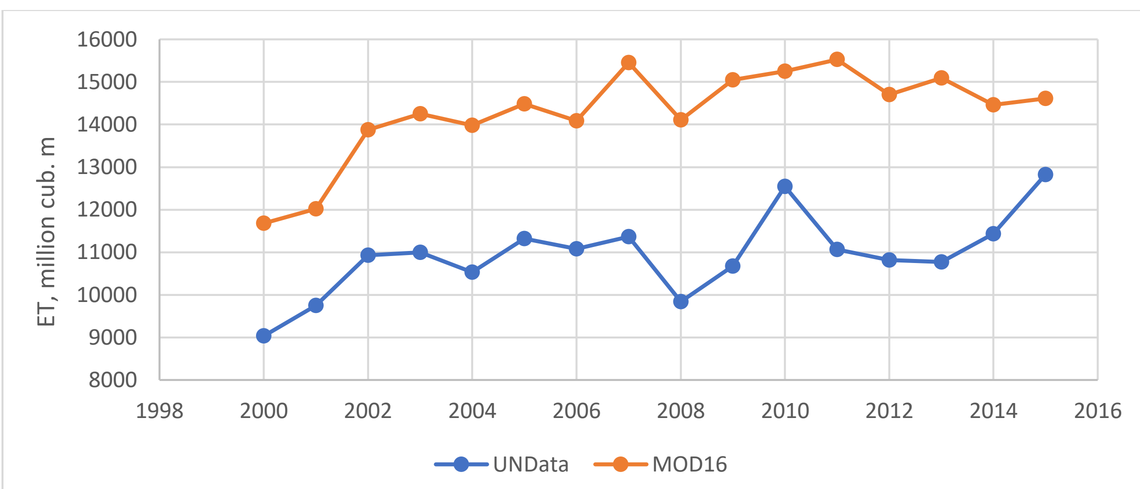

Figure 10. Comparison of Annual Actual Evapotranspiration Values for Armenia obtained from MODIS MOD16 Dataset and presented in UNData Portal

Thus, we can conclude that the different methods have been applied and calculation of ET still has many uncertainties due to its high dependence on land use and climatic characteristics, which are not easy to estimate with sufficient accuracy.

4. Projections of ET and PET Values for 2040, 2070, and 2100

Future changes in annual ET and PET have been projected using the IPCC RCP8.5 scenario (METRAS model).

First, the correlation between precipitation/air temperature and ET/PET have been established.

It has been identified the annual ET values are correlated with annual precipitation, and annual PET values are correlated with annual average air temperature. Calculated values of annual ET and PET, as well as annual average air temperature and annual precipitation data for 2000-2019 have been used for understanding the relationship between those parameters.

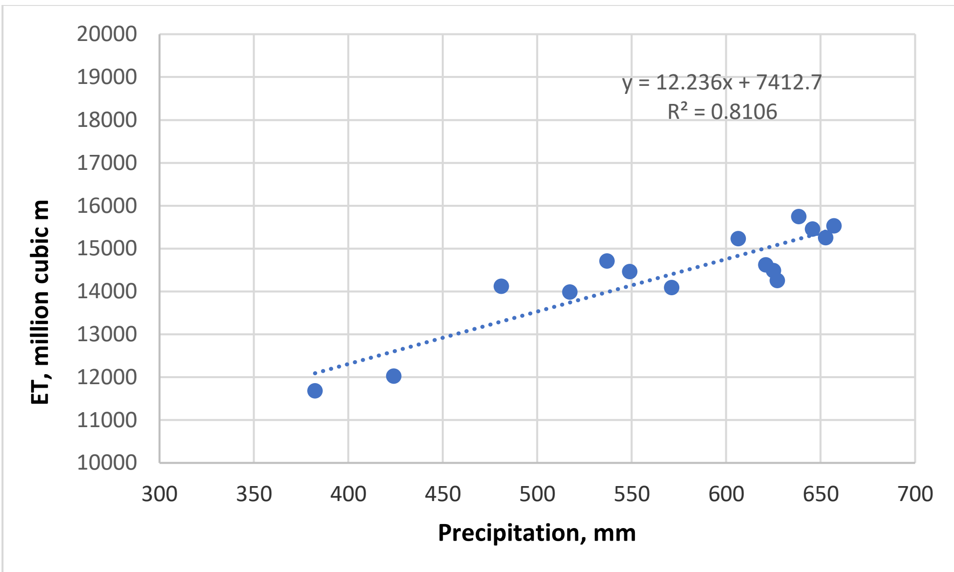

Figure 11. Relationship between annual precipitation and annual actual evapotranspiration

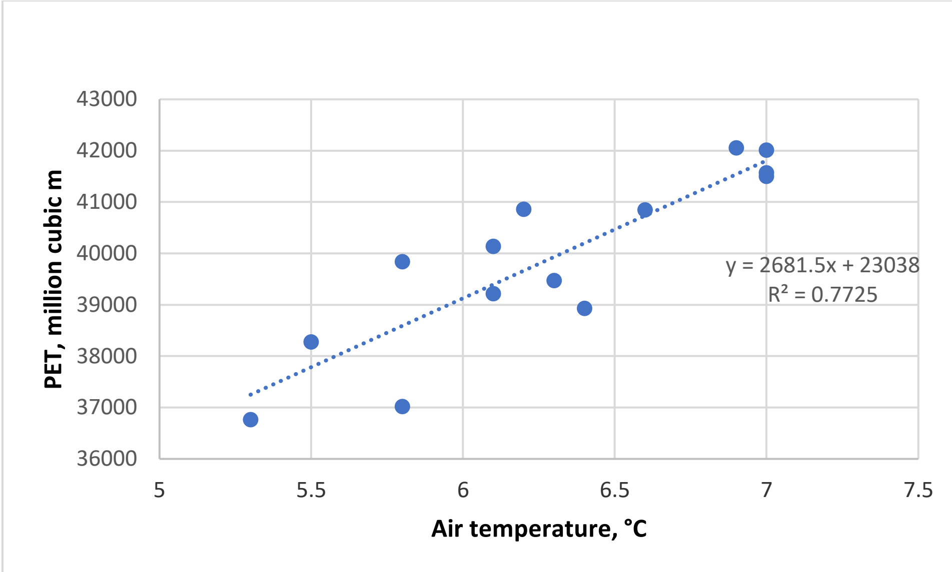

Figure 12. Relationship between annual average air temperature and annual potential evapotranspiration

Using the relationship equations presented in the Figures 11 and 12, the annual actual and potential evapotranspiration have been estimated for 2040, 2070, and 2100 based on the precipitation and air temperature projections for Armenia obtained by METRAS model (Table 5).

Table 5. Projected Values of Annual ET and PET, million cubic meters (RCP8.5 scenario, METRAS model)

Parameter	Average, 2000-2019	2040	2070	2100
ET	14407.3	14460.6	14264.9	14056.8
PET	40164.7	42076.6	46635.2	50389.3

As we can see from the table above, it is projected that the actual evapotranspiration values will decrease. This is due to the forecasted decrease of annual precipitation. Opposite to that, the potential evapotranspiration will increase with the rise of average annual temperature.

The sub-basin-level projections of ET and PET are presented in the Annex 1.

Literature

1. Belward, A. S., Estes, J. E., and Kline, K. D. (1999). The IGBP-DIS global 1-km land-cover data set DISCover: A project overview. *Photogrammetric Engineering and Remote Sensing*, *65*(9), 1013-1020.
2. Bouchet, R. J. (1963). Evapotranspiration reelle, evapotranspiration potentielle, et production agricole. *Ann. agron*, *14*(5), 743-824.
3. Choudhury, B. (2000). A Biophysical Process-Based Estimate of Global Land Surface Evaporation Using Satellite and Ancillary Data. In *Observing Land from Space: Science, Customers and Technology* (pp. 119-126). Springer Netherlands.
4. Choudhury, B. J., & DiGirolamo, N. E. (1998). A biophysical process-based estimate of global land surface evaporation using satellite and ancillary data I. Model description and comparison with observations. *Journal of Hydrology*, 205(3-4), 164-185.
5. Cleugh, H. A., Leuning, R., Mu, Q., and Running, S. W. (2007). Regional evaporation estimates from flux tower and MODIS satellite data. *Remote Sensing of Environment*, *106*(3), 285-304.
6. Courault, D., Seguin, B., and Olioso, A. (2005). Review on estimation of evapotranspiration from remote sensing data: From empirical to numerical modeling approaches. *Irrigation and Drainage systems*, *19*(3-4), 223-249.
7. Dang, Q. L., Margolis, H. A., Coyea, M. R., Sy, M., and Collatz, G. J. (1997). Regulation of branch-level gas exchange of boreal trees: roles of shoot water potential and vapor pressure difference. *Tree Physiology*, *17*(8-9), 521-535.
8. Dawson, T. E., Burgess, S. S., Tu, K. P., Oliveira, R. S., Santiago, L. S., Fisher, J. B., ... and Ambrose, A. R. (2007). Nighttime transpiration in woody plants from contrasting ecosystems. *Tree Physiology*, *27*(4), 561-575.
9. Fisher, J. B., Tu, K. P., and Baldocchi, D. D. (2008). Global estimates of the land–atmosphere water flux based on monthly AVHRR and ISLSCP-II data, validated at 16 FLUXNET sites. *Remote Sensing of Environment*, *112*(3), 901-919.
10. Friedl, M. A., Sulla-Menashe, D., Tan, B., Schneider, A., Ramankutty, N., Sibley, A., and Huang, X. (2010). MODIS Collection 5 global land cover: Algorithm refinements and characterization of new datasets. *Remote Sensing of Environment*, *114*(1), 168-182.
11. Jarvis, P. G. (1976). The interpretation of the variations in leaf water potential and stomatal conductance found in canopies in the field. *Philosophical Transactions of the Royal Society of London B: Biological Sciences*,*273*(927), 593-610.
12. Jiang, L., Islam, S., and Carlson, T. N. (2004). Uncertainties in latent heat flux measurement and estimation: implications for using a simplified approach with remote sensing data. *Canadian Journal of Remote Sensing*, *30*(5), 769-787.
13. Jones, H. G. (1992). *Plants and microclimate: a quantitative approach to environmental plant physiology*. Cambridge university press.
14. Kalma, J. D., McVicar, T. R., and McCabe, M. F. (2008). Estimating land surface evaporation: A review of methods using remotely sensed surface temperature data. *Surveys in Geophysics*, *29*(4-5), 421-469.

15. Kawamitsu, Y., Yoda, S., and Agata, W. (1993). Humidity pretreatment affects the responses of stomata and CO2 assimilation to vapor pressure difference in C3 and C4 plants. *Plant and Cell Physiology*, *34*(1), 113-119.

16. Kelliher, F. M., Leuning, R., Raupach, M. R., and Schulze, E. D. (1995). Maximum conductances for evaporation from global vegetation types.*Agricultural and Forest Meteorology*, *73*(1), 1-16.

17. Leuning, R. (1995). A critical appraisal of a combined stomatal-photosynthesis model for C3 plants. *Plant, Cell & Environment*, *18*(4), 339-355.

18. Los, S. O., Pollack, N. H., Parris, M. T., Collatz, G. J., Tucker, C. J., Sellers, P. J., ... and Dazlich, D. A. (2000). A global 9-yr biophysical land surface dataset from NOAA AVHRR data. *Journal of Hydrometeorology*,*1*(2), 183-199.

19. Marsden, B. J., Lieffers, V. J., and Zwiazek, J. J. (1996). The effect of humidity on photosynthesis and water relations of white spruce seedlings during the early establishment phase. *Canadian Journal of Forest Research*,*26*(6), 1015-1021.

20. Misson, L., Panek, J. A., and Goldstein, A. H. (2004). A comparison of three approaches to modeling leaf gas exchange in annually drought-stressed ponderosa pine forests. *Tree Physiology*, *24*(5), 529-541.

21. Monteith, J. L. (1965). Evaporation and environment. In *Symposia of the Society for Experimental Biology* (Vol. 19, p. 205).

22. Mu, Q., Heinsch, F. A., Zhao, M., and Running, S. W. (2007). Development of a global evapotranspiration algorithm based on MODIS and global meteorology data. *Remote Sensing of Environment*, *111*(4), 519-536.

23. Mu, Q., Zhao, M., and Running, S. W. (2011). Improvements to a MODIS global terrestrial evapotranspiration algorithm. *Remote Sensing of Environment*, *115*(8), 1781-1800.

24. NASA Earth Observing System MODIS Land Algorithm (For Collection 6).

25. Oren, R., Sperry, J. S., Katul, G. G., Pataki, D. E., Ewers, B. E., Phillips, N., and Schäfer, K. V. R. (1999). Survey and synthesis of intra-and interspecific variation in stomatal sensitivity to vapour pressure deficit.*Plant, Cell & Environment*, *22*(12), 1515-1526.

26. Pidwirny, M. (2006). "Actual and Potential Evapotranspiration". *Fundamentals of Physical Geography, 2nd Edition*. Date Viewed. http://www.physicalgeography.net/fundamentals/8j.html

27. Running, S. W., and Kimball, J. S. (2005). Satellite-Based Analysis of Ecological Controls for Land-Surface Evaporation Resistance. *Encyclopedia of hydrological sciences*.

28. Running, S. W., Loveland, T. R., and Pierce, L. L. (1994). A vegetation classification logic based on remote sensing for use in global scale biogeochemical models. *Ambio, 23*, 77-81.

29. Running, S. W., Mu, Q., Zhao, M., and Moreno, A. (2019) User's Guide: MODIS Global Terrestrial Evapotranspiration (ET) Product (MOD16A2/A3 and Year-end Gap-filled MOD16A2GF/A3GF)

30. Running, S. W., Nemani, R. R., Heinsch, F. A., Zhao, M., Reeves, M., and Hashimoto, H. (2004). A continuous satellite-derived measure of global terrestrial primary production. *Bioscience*, *54*(6), 547-560.

31. Salehnia, N., Kolsoumi, S., Rahman, M., Ullah, A., Pezeshki, A., Banezhad, B., and Mirzadeh, J. (2018). Calculation Actual and Potential Evapotranspiration by developing a Tool for MODIS Product.

32. Sandford, A. P., and Jarvis, P. G. (1986). Stomatal responses to humidity in selected conifers. *Tree Physiology*, *2*(1-2-3), 89-103.

33. Schubert, S. D., Rood, R. B., and Pfaendtner, J. (1993). An assimilated dataset for earth science applications. *Bulletin of the American meteorological Society*, *74*(12), 2331-2342.

34. Schulze, E. D., Kelliher, F. M., Korner, C., Lloyd, J., and Leuning, R. (1994). Relationships among maximum stomatal conductance, ecosystem surface conductance, carbon assimilation rate, and plant nitrogen nutrition: a global ecology scaling exercise. *Annual Review of Ecology and Systematics*, 629-660.

35. Shuttleworth, W. J., and Wallace, J. S. (1985). Evaporation from sparse crops-an energy combination theory. *Quarterly Journal of the Royal Meteorological Society*, *111*(469), 839-855.

36. Sulla-Menashe, D., Gray, J. M., Abercrombie, S. P., & Friedl, M. A. (2019). Hierarchical mapping of annual global land cover 2001 to present: The MODIS Collection 6 Land Cover product. *Remote Sensing of Environment*, 222, 183-194.

37. Thornton, P.E. (1998). Regional ecosystem simulation: combining surface- and satellite-based observations to study linkages between terrestrial energy and mass budgets. PhD. Dissertation, School of Forestry, *The University of Montana*, Missoula, MT., 280 pp.

38. Tuzet, A., Perrier, A., and Leuning, R. (2003). Stomatal control of photosynthesis and transpiration: Results from a soil–plant–atmosphere continuum model. *Plant, Cell and Environment*, *26*, 1097-1116.

39. van de Griend, A. A., and Owe, M. (1994). Bare soil surface resistance to evaporation by vapor diffusion under semiarid conditions. *Water Resources Research*, *30*, 181-188.

40. Wan, Z., Zhang, Y., Zhang, Q., and Li, Z. L. (2002). Validation of the land-surface temperature products retrieved from Terra Moderate Resolution Imaging Spectroradiometer data. *Remote sensing of Environment*, *83*(1), 163-180.

41. White, M. A., Thornton, P. E., Running, S. W., and Nemani, R. R. (2000). Parameterization and sensitivity analysis of the BIOME-BGC terrestrial ecosystem model: net primary production controls. *Earth interactions*, *4*(3), 1-85.

42. Xu, L., and Baldocchi, D. D. (2003). Seasonal trends in photosynthetic parameters and stomatal conductance of blue oak (Quercus douglasii) under prolonged summer drought and high temperature. *Tree Physiology*, *23*(13), 865-877.

43. Zhao, M., Heinsch, F. A., Nemani, R. R., and Running, S. W. (2005). Improvements of the MODIS terrestrial gross and net primary production global data set. *Remote Sensing of Environment*, *95*(2): 164–176.

44. Zhao, M., Running, S. W., and Nemani, R. R. (2006). Sensitivity of Moderate Resolution Imaging Spectroradiometer (MODIS) terrestrial primary production to the accuracy of meteorological reanalyses. *Journal of Geophysical Research*, *111, G01002*, doi:10.1029/2004JG000004